

# Simulation of the Effects of Spark Timing and External EGR on Gasoline Combustion Under Knock-Limited Operation at High Speed and Load

Michal Pasternak<sup>1</sup>(✉), Corinna Netzer<sup>1</sup>, Fabian Mauss<sup>1</sup>,  
Michael Fischer<sup>2</sup>, Marc Sens<sup>3</sup>, and Michael Riess<sup>3</sup>

<sup>1</sup> Brandenburg University of Technology, Cottbus, Germany  
{michal.pasternak, corinna.netzer, maussf}@b-tu.de

<sup>2</sup> Tenneco GmbH, Edenkoben, Germany  
mfischerl@tenneco.com

<sup>3</sup> IAV GmbH, Berlin, Germany  
{marc.sens, michael.riess}@iav.de

**Abstract.** Combustion in a spark ignition engine operated at high speed and load is investigated numerically with regard to knock behavior. The study focuses on the concurrent impact of spark timing and exhaust gas recirculation (EGR) on the severity of knock. Specifically, the possibility of knock reduction through the lowering of nitrogen oxide (NO) content in the rest-gas is examined. Simulations are carried out using a stochastic reactor model of engine in-cylinder processes along with a quasi-dimensional turbulent flame propagation model and multicomponent gas-phase chemistry as gasoline surrogate. The knock-limited conditions are detected using the detonation diagram. By lowering the NO content in the external EGR the end-gas auto-ignition is suppressed. This prevents a transition to knocking combustion and enables advancing of spark timing that yields better combustion phasing. As a result, fuel economy is improved and the potential benefits of cleaning the EGR are indicated.

## 1 Introduction

Meeting the ever tightening emission standards and future fuel economy demands are the driving forces behind the development of high-efficiency combustion engines. In the context of spark ignition (SI) gasoline engines, the development efforts are frequently targeted at improving the resistance to knocking combustion that is one of the major cause of rather poor thermal efficiency of SI engines. The tendency for knock prevents an optimum combustion phasing and high compression ratio that along with mixture specific ratio govern thermal efficiency of gasoline engines. Besides deteriorating thermal efficiency and consequently also increasing fuel consumption, the knocking combustion increases exhaust emissions and may cause a damage of engine hardware [1, 2].

Commonly accepted theories assume engine knock to be an abnormal combustion (see, e.g. [2–8] that underlie the description in this section). It results from a spontaneous auto-ignition of a portion or portions of the end-gas air-fuel mixture that occur ahead of the propagating flame front and if the associated release of chemical energy is sufficient to cause the formation of pressure waves of substantial amplitude and frequency. The occurrence of pressure waves is revealed by a characteristic metallic noise with a frequency between 10–30 kHz [3] referred to as knock. Auto-ignition is the primary process for the development towards knocking combustion. It does not happen well distributed within the end-gas region, but in localized spots entrapped inside the heterogeneous area in front of the propagating flame. These so called exothermic centers with specific induction time and specific excitation characteristic (spatial and temporal heat release) emerge from incomplete mixing and temperature inhomogeneity. Whether a self-ignition in the end-gas region will develop into what is referred to as engine knock is dependent on the properties of the exothermic centers, such as size gradient and spatial distribution [4]. These properties determine the magnitude of the heat released by the exothermic center and hence, also the magnitude of the resulting pressure oscillations.

Most commonly, the detection and analysis of knock are carried out based on the measured in-cylinder pressure data or acoustic signals by means of acceleration sensors mounted to the engine crankcase. These methods indicate the occurrence of knock, but provide no information about its phenomenology. This drawback is avoided in the complex and expensive optical methods. These methods enable the detection of intermediate species and radicals that are markers of auto-ignition. They may also provide the time and space resolved information about the flame development. Hence, they contribute to better understanding of the transition from auto-ignition to knocking combustion. Further support of the analysis of knock and its detection is offered by numerical simulations. Here, one can list simple zero-dimensional (0D) or one-dimensional (1D) approaches and complex three-dimensional (3D) computational fluid dynamics (CFD) (see, e.g. [8, 9]). All these methods become particularly robust if coupled with chemical kinetic models that enable the prediction of end-gas auto-ignition that initiates knocking combustion.

Because of the negative effects of knock on the combustion process of SI engines, significant efforts are being made to develop methods of its suppression. Classically, the tendency for knock has been avoided by retarding the spark timing towards the expansion stroke or by reducing the compression ratio. However, both these methods deteriorate thermal efficiency. Furthermore, late combustion phasing increases exhaust gas temperature that at high loads may significantly increase thermal loading and cause engine damage. To avoid this drawback, mixture enrichment is frequently applied that in turn influences negatively fuel economy. Among other methods of knock suppression one can list [2, 5, 8, 10] increasing turbulence and combustion speed, application of cooled exhaust gas recirculation (EGR) and dedicated EGR composition, direct fuel injection, water injection, variable valve timing, developing of fuels with anti-knocking performance, such as liquefied petroleum gas fuels, increasing fuel octane index by using variety of antiknock additives or the reduction of nitrogen oxide (NO) content in the rest-gas.

Among the listed above methods, so far relatively less work has been devoted to the possibility of knock suppression by the reduction of NO contained in the rest-gas. The increased reactivity of the air-fuel mixture in the presence of even trace amounts of NO is known from the literature [11, 12]. The negative impact of NO on auto-ignition tendency and knock in SI engines has already been indicated in [13–15] and more recently in [16, 17]. To our best knowledge, the work reported in [14] is the most thorough numerical analysis of the chemical impact of NO on the end-gas auto-ignition in SI engines. In that work, calculations were carried out using a simple two-zone and homogeneous model of SI combustion along with a reaction mechanism for primary reference fuel (PRF) as gasoline surrogate. In some extent, the present work can be considered as a further development of that in [14]. However, here simulations are carried out with consideration for mixture inhomogeneity due to the impact of fuel injection, heat transfer and turbulent mixing. Thus, the effects of temperature fluctuations and inhomogeneity, which are present in the gas mixture in actual engines [18], are respected in the model. Furthermore, a multicomponent reaction mechanism is employed. In contrast to the commonly used PRF models, here we respect also the impact of ethanol and aromatic contents that enable better representation of fuels used in actual SI engines. Overall, the present approach provides a modeling framework that is tailored for the simulation of modern SI engines with direct fuel injection.

The specific purpose of this article is to provide a parametric analysis of combustion to explore the potential of knock suppression throughout the reduction of NO in the external EGR. The reduction of NO is carried out with respect to the possibility to optimize combustion phasing and hence, to improve fuel economy while operating the engine at the knock limit. The analysis deals with a gasoline engine that is operated at high load and speed and with cooled EGR. The rest part of the article is structured as follows. Firstly, a brief description of the numerical model is given. Next, the applied experimental and numerical methods of knock detection are presented. Subsequently, the modeling framework and assumptions are discussed. Finally, exemplary simulation results are presented and the work is summarized.

## 2 Modeling Approach

The modeling approach adopted for the present study features a stochastic reactor model (SRM) of in-cylinder processes in SI engines along with a turbulent flame propagation model and multicomponent model of gas-phase chemistry as gasoline surrogate. The models belong to the LOGEngine [19] simulation platform that is specifically tailored to the simulation of physical and chemical processes in combustion engines. Below, a basic description of each model is presented for readability of the article. The description has been freely adopted from our previous works [19–21] that contain thorough description of the sub-models.

### 2.1 Stochastic Reactor Model

The SRM is a 0D model of physical and chemical processes occurring in combustion engines during the closed part of the engine cycle. It is formulated within a probability

density function (PDF) approach for the simulation of turbulent flows with chemical reactions. For SI engines, the SRM is formulated as two-zone model; burned and unburned zones are distinguished that result from the flame propagation across the combustion chamber. There is no interaction between the zones except for the transfer of mass as the combustion proceeds. The gas inside each zone is treated as an ensemble of notional particles. Each zone is assumed to be statistically homogenous, and particle-particle interaction is purely stochastic. Particles can mix with each other and exchange heat with the cylinder walls. Each particle has a chemical composition, temperature and mass and hence, each particle represents a point in phase-space for species mass fraction and temperature. These scalars are treated as random variables and can vary within the cylinder. They determine the composition of the gas mixture and are described with probabilities using PDFs. The frequency of scalar mixing between particles is governed by the mixing time that is explained in the next section. Mixing time is the main modeled parameter for the SRM. By its modeling, the inhomogeneity is introduced into the gas-phase for species concentration and temperature. Besides the impact of mixing, the mixture inhomogeneity is further enhanced by the heat transfer to the wall and fuel injection. Overall, the modeled inhomogeneity of the mixture mimics, in some extent, the turbulence effects in actual engines.

## 2.2 Turbulent Flame Propagation and Mixing Time

The SRM employs a quasi-three dimensional turbulent flame propagation model that governs the mass transfer from the unburned zone to the burned zone. A spherically expanding flame is assumed that is limited by the cylinder walls. The turbulent flame speed ( $S_T$ ) is calculated after [22] based on the laminar flame speed ( $S_L$ ) and turbulent intensity that is represented by the velocity fluctuations ( $u'$ ).

$$S_T/S_L = 1 + C(u'/S_L)^m \quad (1)$$

Here,  $C$  and  $m$  are constants and equal to 2.5 and 0.9, respectively. The  $S_L$  is taken from a pre-generated library for pure iso-octane and for different pressures, temperatures, equivalence ratios and EGR rates. The value of  $u'$  is calculated as the ratio between the integral length scale ( $l_I$ ) of the flow and the turbulent mixing time ( $\tau_t$ ) that represents the time taken to transfer the turbulent kinetic energy ( $k$ ) from the large scales to small scales, where due to viscosity it is dissipated ( $\varepsilon$ ) into heat. Hence, the turbulent flame propagation is calibrated by only the turbulent mixing time.

$$\tau_t = l_I/u' \cong k/\varepsilon \quad (2)$$

The turbulent flame speed is assumed to be constant in all directions unless the flame encounters a barrier. The geometric effects of near-wall flame quenching on the flame shape are not modelled.

With respect to the SRM simulations, rather than the turbulent mixing time the scalar mixing time is used. For simplicity, it is called in the later part of this article just as mixing time and is denoted by  $\tau$ . The mixing time used in the SRM is related to the turbulent mixing time,  $\tau_t$ , by the mixing time constant  $C_\phi$  (see, e.g., [23]).

$$\tau = C_{\phi}^{-1} \tau_t \quad (3)$$

The constant  $C_{\phi}$  is interpreted as velocity-scalar decay time scale. Knowing an overall trend of  $\tau_t$  and calibrating  $C_{\phi}$ , the right-hand side of Eq. (3) can be determined and it models the mixing time that is used as an input for the SRM.

### 2.3 Reaction Kinetics for Gasoline Surrogate

A four component reaction kinetics mechanism from LOGEfuel [19] has been used as gasoline surrogate. The mechanism has been successfully used in our recent work [24] devoted to the analysis of combustion in SI engines. It contains sub-models describing the oxidation process of ethanol, toluene, iso-octane and n-heptane and is referred to as ethanol-toluene reference fuel (ETRF). The mechanism contains also the thermal model of NO formation and growth pathways for polyaromatic hydrocarbons that are compatible with the soot model used in the LOGEEngine platform. The version of the mechanism used in the present study contains 193 species and 2088 reactions. The content of ethanol, toluene, iso-octane and n-heptane was set to 0.15, 0.39, 0.29 and 0.17, respectively and on a mole fraction basis. For such defined mixture the research octane number (RON) index is 91 and lower heating value (LHV) is 41.6 MJ/kg. These values match exactly with the values reported for the fuel used during the experimental work; the exact composition of the fuel used during the experimental work was unknown.

## 3 Detection of Knocking Combustion

The detection of engine knocking combustion and subsequently the determination of engine operating conditions at the knock limit underlie all investigations presented in this article. They were carried out separately for both simulated and measured data.

### 3.1 Experimental Method for Engine Knock Detection and Control

In the development of combustion engines, the precise measurement of the in-cylinder pressure with a high temporal and signal resolution via quartz-crystal pressure transducers is a standard. In this work, the knock indicator system from IAV (KIS4) was employed in order to identify knocking combustion [25, 26]. The system uses the in-cylinder pressure signal from a quartz-crystal sensor that is analyzed in the time domain. In Fig. 1 the signal chain inside KIS4 is presented. The cylinder and cycle individual maximum peak of the high pass filtered and rectified pressure, which is denoted by PS, is used to describe the severity of engine knock.

In order access whether each individually recorded and analyzed cycle is knocking or not, the peak pressure PS is set in relation to a normative. This normative or threshold might be different for each engine and is application tailored. Frequently, the knock threshold is set to consider the background noise in the in-cylinder pressure

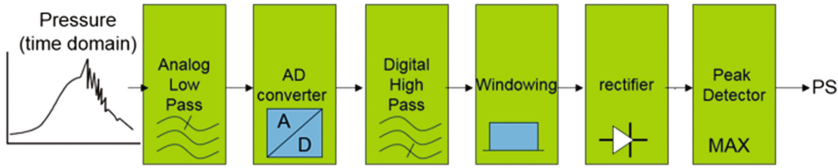


**Fig. 1.** Overview of pressure signal conversion in KIS4

signal coming along with an increase of engine speed. Thus, a typical empirical definition of the maximum pressure  $PS$  allowed for a cycle to be judged not knocking is to undercut the logic:  $PS < \text{engine speed}/2000$ , where the right hand side of the inequality defines the knock threshold. This definition was also employed in the present work. In order to account for the stochastic nature of engine knock, a statistical validation of the analyzed  $PS$  data is performed. Typically, the spark timing on the engine test bench is controlled to allow a certain percentage of cycles to be the knocking cycles according to the defined knock threshold. It is assumed that the knock limit is achieved if for 2% of the analyzed cycles the  $PS$  is greater than the assumed knock threshold.

### 3.2 Knock Detection During Simulations

As stated in the introduction section, according to the commonly accepted theories the occurrence of auto-ignition of the end-gas mixture is a necessary but not sufficient condition to give rise to knocking combustion [27, 28]. To cope with this issue, in the present work we adopt a concept of developing detonation to determine the occurrence of knock and to define engine operating conditions at the knock limit. Overall, the concept assumes that the developing detonation, which is associated with the presence of pressure waves and follows the auto-ignition, may occur if the chemical and acoustic waves reinforce each other and if the gas mixture is sufficiently reactive [28]. The foundation of the concept is dated back to the work reported in [29], where different modes of a propagating chemical reaction in the reactive mixture are distinguished. This concept was extended in [28, 30] and resulted in a theory of wave reinforcement. In [31], the occurrence of hot-spots causing temperature gradients was added to the auto-ignition concept. These concepts were further investigated and extended in [32, 33] with reference to the analysis of super-knock.

For the analysis of different modes of developing detonation that follows the auto-ignition with hot-spots, detonation diagrams are frequently applied. The concept of a detonation diagram was introduced in [28] and was also used in our recent work [24]. In the detonation diagram the evolution of an ignition to a developing detonation, which is understood as knocking combustion, is described using two dimensionless parameters  $\zeta$  and  $\varepsilon$  that after [34] are referred to as resonance parameter and reactivity parameter, respectively. The parameter  $\zeta$  is calculated as the ratio between the speed of sound,  $a$ , and the reaction velocity,  $u$ . This ratio determines if the two waves are in the same order of magnitude and therefore, may combine and grow to a developing detonation or if the reaction front will travel at subsonic or supersonic speed. The reaction velocity can be determined from the temperature,  $T$ , and the ignition delay time,  $\tau_i$  [31].

$$\xi = u/a = a(\partial T/\partial x)(\partial \tau_i/\partial T) \quad (4)$$

The reactivity parameter  $\varepsilon$  is determined by the ratio of the constant temperature kernel length  $l$  and the length that the speed of sound travels during the ignition event. Thus, it is a measure of the reactivity and the size of the ignition kernel [31].

$$\varepsilon = l/(a \cdot \tau_e) \quad (5)$$

Here,  $\tau_e$  is the excitation time that denotes time between 5% of heat release until the maximum heat release during the ignition. As  $\varepsilon$  increases, the range of  $\xi$ , which can lead to a developing detonation, also increases that results in a characteristic peninsula bounded by the solid lines in Fig. 2 (results elaborated from [28, 35, 36]). The upper limit of the peninsula is denoted by  $\xi_u$  and the lower limit by  $\xi_l$ . Overall, the  $\varepsilon$ - $\xi$  solution indicates about the pressure development mode. Besides the peninsula of developing detonation, the remaining three regimes based on  $\xi$  and  $\varepsilon$  values are deflagration, subsonic auto-ignition and thermal explosion [36]. The transition from the subsonic auto-ignition to the developing detonation is most interesting from the point of view finding operating conditions at knock limit.

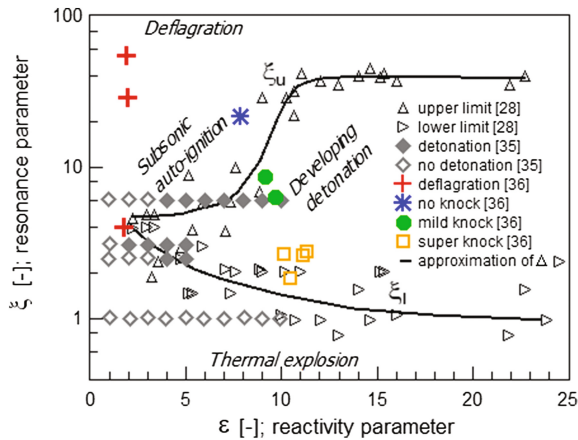


**Fig. 2.** The parameters  $\varepsilon$ - $\xi$  defining the detonation peninsula (solid lines, [28]) and indicating different modes of reaction front propagation (elaborated from [28, 35, 36])

The detonation diagram was first developed for syngas mixtures [28, 30]. In [35], it was verified that the boundaries for detonation (Fig. 2) are also valid for other fuels, such as n-heptane and iso-octane, since the developing detonation depends on the high temperature chemistry. In [36] and references therein reported, engine-relevant-regimes were defined on the detonation diagram (Fig. 2) and based on the 3D large eddy simulations.

The methodology reported in [28, 30–33] for the calculation of parameters  $\xi$  and  $\varepsilon$  has been transferred to the SRM and is discussed in detail in [24]. Here we summarize

this methodology for readability of the article. The methodology is based on the analysis of heat release and the local conditions in the unburned zone and is applied in a post-process. Since there is no spatial resolution for the particles, all particles that contribute to the investigated high temperature peak are collected and treated as one ignition kernel that is assumed to be a sphere. To determine the maximum knock intensity of the current cycle, all particles are selected that have their maximum heat release in the same time step as the maximum gradient in the rate of heat release that is calculated for the entire in-cylinder mixture. Particles that ignite in an earlier or later time step are accounted to a different auto-ignition kernel. In this way, the most severe auto-ignition event (steepest heat release gradient) of the current cycle is investigated and evaluated. Due to the auto-ignition, the temperature of the kernel is increased and hence, the volume also increases accordingly. The difference between the radius of the ignition kernel before and after the ignition gives the length  $x$  that is needed for Eq. (4). The gradient of ignition delay time,  $\tau_i$ , is calculated using the maximum particle temperature that is included in the ignition kernel before the ignition occurs and using the mean temperature of the unburned zone. The speed of sound is calculated as a function of the mean properties of the end gas. The excitation time is calculated analogously to the calculation of ignition delay time. Fuel characteristics, such as ignition delay time and excitation time, are calculated using a constant volume reactor from [19].

## 4 Computational Set-up and Method

### 4.1 Engine Layout and Operating Points

The computational analysis is carried out for a 1.4 L, four-cylinder, direct injection, 16-valve, turbocharged SI engine that is operated with external EGR. The engine is fueled with standard gasoline fuel that is characterized by RON 91. The basic specification of the engine is summarized in Table 1.

**Table 1.** Engine basic specification

Parameter	Value
Bore [mm]	74.5
Stroke [mm]	80
Compression ratio [-]	9.7
Connecting rod [mm]	140

Two operating points, which are defined by engine speed and load, are used in this study. Their basic characteristic is given in Table 2.

The operating point OP1 is used to verify the predictive capability of the SRM in the context of simulating spark timing (ST) sweep. For this operating point the measured in-cylinder pressure was available for three different spark timing positions, namely  $-6$ ,  $-3$  and  $0$  crank angle degrees (CAD) after top dead center (ATDC). The



**Table 2.** Engine operating points

Parameter	OP1	OP2
Engine speed [1/min]	1750	4750
IMEP [bar]	16	17
Equivalence ratio [-]	1.0	1.0

operating point OP2 is the main point for the analysis of the impact of NO reduction in the rest-gas on the suppression of knock. At this operating point the engine is operated at knock limit. According to the measurement methodology described in Sect. 3.1, it means that knocking combustion occurred in 2% out of 500 measured pressure cycles. Furthermore, at OP2 the engine is operated with 7.9% of external EGR.

## 4.2 SRM Set-up and Procedure

The SRM is applied to simulate combustion and tendency for knocking during the closed part of the engine cycle, between inlet valve closure (IVC) and exhaust valve opening (EVO). The in-cylinder mixture is discretized into 1000 particles. Calculations are carried out with 0.5 CAD time step. The detailed ETRF model outlined in Sect. 2.3 is used as gasoline surrogate.

The initial conditions for the SRM are calculated using a method implemented in the LOGEngine platform. The method employs a genetic algorithm to find the parameters at IVC, such as initial mass and temperature, mixture composition, internal EGR and absolute pressure. The apparent rate of heat release is used as a reference and target parameter during the analysis. The algorithm employs detailed chemistry through the calculation that enables accurate representation of the initial gas composition.

The SRM is calibrated using a crank angle dependent mixing time ( $\tau$ ) that is optimized until the simulated engine parameters, such as in-cylinder pressure and rate of heat release, match the experimental counterparts. The optimization is carried out using the LOGEngine. The history of mixing time is modeled as a combination of linear and exponential function [19]. The modeling is targeted at mimicking the changes of mixing time that usually are seen in 3D CFD solutions (see, e.g. [21]) and based on Eq. (2). The modeled mixing time maps the impact of the 3D character of actual in-cylinder processes into the 0D domain of the SRM.

Several assumptions have been made to isolate the impact of NO contained in the rest-gas on the auto-ignition tendency and knock. The rest-gas is assumed to be composed of nitrogen ( $N_2$ ), carbon monoxide (CO), carbon dioxide ( $CO_2$ ), water steam ( $H_2O$ ) and NO. Such a composition was obtained during the preliminary calculations as an average composition from the multi-cycle simulations using the SRM. The concentration of CO,  $CO_2$  and  $H_2O$  in the rest-gas is kept constant for all calculations carried out in this work. The changes of NO content are suitably compensated by an increase or decrease of  $N_2$  content. The impact of cycle to cycle variation on the in-cylinder pressure and knock tendency is not considered here. The possible impact of stochastic mixing, heat transfer and fuel injection on the combustion rate and knocking

tendency is eliminated by representing these parameters as means calculated over thirty consecutive cycles; the rest-gas composition still remains unchanged for each cycle. Overall, all computed results are understood as coming from a single representative cycle for a given set of initial and operating conditions.

### 4.3 Model Extrapolation for Varied Spark Timing

The possibility to predict engine in-cylinder parameters, such as rate of heat release and pressure, for varied spark timing is crucial for the overall performance of the model. It enables an estimation of the concurrent impact of reducing NO in the rest-gas and advancing of spark timing on the combustion process. In the present work, the predictive capability of the SRM is obtained through the calibration of mixing time history at a given operating point and subsequently, its extrapolation to different ST positions at that operating point.

Overall, mixing time varies according to the variation of turbulent kinetic energy that in turn is affected by engine geometry and depends strongly on engine speed (see, e.g. [21] and references therein). Hence, for a varied spark timing, and if the engine speed does not change, it is assumed that the history of mixing time also remains unchanged. Only the anchorage of mixing time history (see the profiles in Fig. 3) on a crank angle basis has to be extrapolated according to the ST changes.

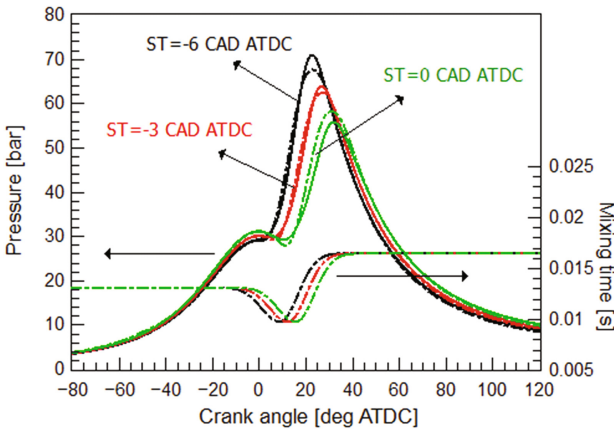


**Fig. 3.** Experimental (solid lines) and simulated (dash-dotted lines) pressure histories for different STs along with the calibrated mixing time history for ST = -3 CAD ATDC and the extrapolated histories for ST = -6 and 0 CAD ATDC (results for OP1:  $n = 1750$  rpm and IMEP = 16 bar)

The performance of the proposed modeling of mixing time extrapolation is demonstrated based on the calculations carried out for OP1 (Table 2). For this OP the engine speed ( $n$ ) is 1750 rpm and indicated mean effective pressure (IMEP) is 16 bar. Thus it is rather low speed but high load operating point. The experimental pressure data for this OP are available for three ST positions, namely -6, -3 and 0 CAD ATDC.

The SRM was calibrated for  $ST = -3$  CAD ATDC. To predict in-cylinder performances at  $ST$  equal to  $-6$  and  $0$  CAD ATDC, the mixing time history is moved by  $3$  CAD receptively to the earlier and later positions during the cycle. More specifically, only the nonlinear part of the mixing time history shown in Fig. 3, in between  $-10$  and  $40$  CAD ATDC is moved; this regime corresponds approximately to the duration of combustion. The results from the calibrated and extrapolated SRM are presented in Fig. 3 for in-cylinder pressure and in Fig. 4 for combustion progress. The combustion progress is defined by crank angles corresponding to 10%, 50% and 90% of the total energy release during combustion. These characteristic CA positions are denoted as CA10, CA50 and CA90, respectively.

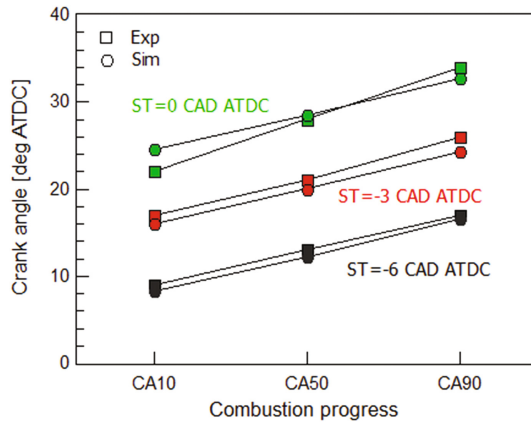


**Fig. 4.** Computed (circles) and experimentally obtained (squares) CA10, CA50 and CA90 for different  $ST$  positions for the engine operated at OP1 with  $n = 1750$  rpm and  $IMEP = 16$  bar

Using mixing time as the only calibration parameter, the simulated pressure histories and combustion progress match well the experimental counterparts. Some small deviations observed at  $ST = 0$  CAD ATDC for CA10 and CA90 indicate that besides extrapolating mixing time with respect to  $ST$  position it may also be beneficial to extrapolate its values. This may help to improve the accuracy of the model for very early and late phases of combustion. Overall, the accuracy of the obtained results is sufficient with respects to the objectives of the present work. For this reason, the outlined methodology of mixing time extrapolation is also applied in Sect. 5 that discusses the impact of NO contained in the rest-gas on the combustion process.

## 5 Results and Discussion

The analysis of the interaction between  $ST$  and NO content in the rest-gas is carried out for OP2 (Table 1) that is operated at the knock limit and at  $n = 4750$  rpm and  $IMEP = 17$  bar. The  $ST$  for this operating point equals  $-9$  CAD ATDC and is denoted as the reference position ( $ST_{ref}$ ). The initial NO content in the in-cylinder mixture,

which was found during the preliminary tests, is 330 ppm. This combination of NO and ST is referred to in this work as the baseline configuration. First, the quality of the model calibration is discussed. Then, the determination of knock limit is presented. Subsequently the impact of ST changes and NO content in the rest-gas on the combustion progress and knocking tendency are presented. Finally, the possibility to reduce fuel consumption through the concurrent reduction of NO content in the rest-gas and advancing ST is demonstrated.

## 5.1 Numerical Model Calibration

The combustion process simulated by the SRM is verified quantitatively by the comparison of the computed in-cylinder pressure and rate of heat release (RoHR) histories to the measured data (Fig. 5). The calibration process is based on mixing time calibration and it follows the methodology outlined in Sect. 4.2. Overall, there is a good agreement between the simulated and measured quantities and hence, the SRM is assumed to be calibrated with respect to the combustion process.

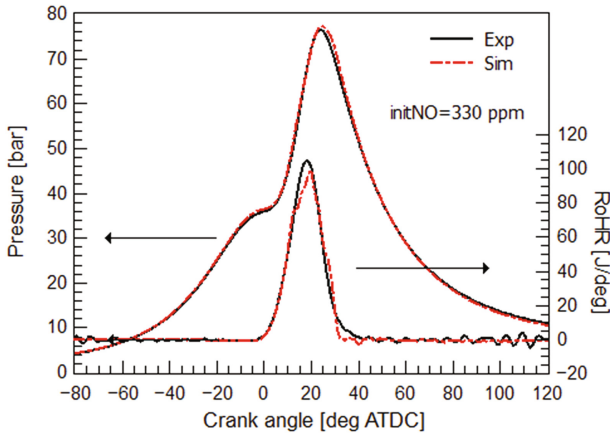


**Fig. 5.** Experimental (solid line) and computed (dash-dotted line) histories of in-cylinder pressure and rate of heat release for OP2 ( $n = 4750$  rpm, IMEP = 17 bar, 330 ppm of initial NO)

## 5.2 Engine Operation at Knock Limit

To verify if the simulated pressure and RoHR data in Fig. 5 correspond to the operation at knock limit, the rate of heat release in the unburned zone is analyzed. Furthermore, the solution from the SRM, in the form of non-dimensional resonance parameter,  $\varepsilon$ , and reactivity parameter,  $\zeta$ , is mapped over the detonation limits as presented in Sect. 3.2. In the baseline configuration ( $ST_{ref}$  and results in Fig. 5), the history of RoHR-u (solid line in Fig. 6a) shows two characteristic peaks due to low and high temperature chemistry, respectively. Both peaks are of the same order of magnitude. This indicates that the end-gas has mainly a low temperature that may not give rise to knock. A confirmation of it is given by the  $\varepsilon$ - $\zeta$  solution (circle in Fig. 6b) that is found shortly before the upper limit of detonation ( $\zeta_u$ ).

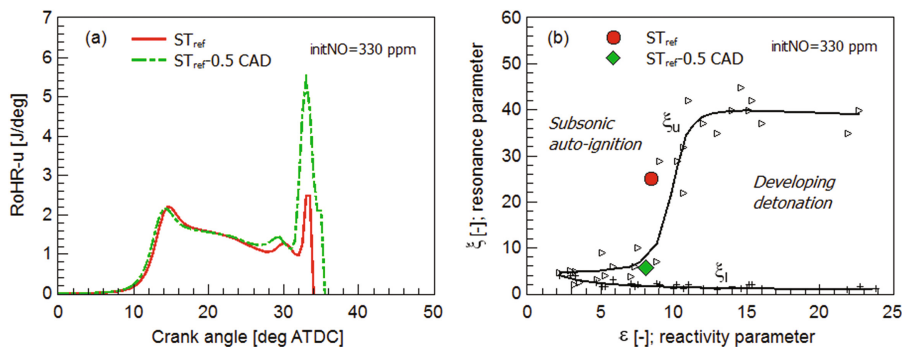


**Fig. 6.** Computed RoHR-u histories (a) and  $\varepsilon$ - $\xi$  solutions (b) in the detonation diagram from [28] for the engine operated at OP2 with 330 ppm of initial NO in the mixture for not-knocking conditions at  $ST_{ref}$  and for knocking conditions at  $ST_{ref} - 0.5$  CAD

In order to check if the obtained solution corresponds indeed to the knock limit, the spark timing is advanced by 0.5 deg ( $ST_{ref} - 0.5$  deg) from the baseline position. The ST has been selected since it is one of the most sensitive parameters for the occurrence of knock. The RoHR-u history and  $\varepsilon$ - $\xi$  solution after the advancing of ST are represented by dash-dotted line in Fig. 6(a) and filled diamond in Fig. 6(b), respectively. The advancing of ST just by 0.5 deg changes the conditions in the end-gas significantly. The second peak in the RoHR-u history, which is due to the high temperature chemistry, is now significantly higher than the peak resulting from the low temperature chemistry. This behavior is reflected in the detonation diagram by the  $\varepsilon$ - $\xi$  solution being within the peninsula of developing detonation, between the  $\xi_l$  and  $\xi_u$ . Thus, knocking combustion is indicated for these conditions. Therefore, we consider the simulated results for  $ST_{ref}$  as corresponding to the knock limit. This evaluation agrees with the evaluation obtained from the measured in-cylinder pressure signal and using the method presented in Sect. 3.1.

### 5.3 Combustion Phasing Effects

To further demonstrate the impact of ST changes on the auto-ignition and knocking tendency, the calculations are carried out for six different ST values that are listed in Fig. 7. The calculations refer to 287 ppm of NO in the initial mixture. Starting from  $ST = -9$  CAD ATDC, the mixing time histories for other ST positions are obtained by following the methodology described in Sect. 4.3. By advancing the ST, the start of combustion, combustion center (CA50) and maximum peak pressure occur earlier during the cycle. This is an expected tendency and hence, the predicted results are considered plausible.

Through the analysis of RoHR-u and the  $\varepsilon$ - $\xi$  solution on the detonation diagram, the results presented in Fig. 7 are quantitatively diagnosed with respect to the occurrence of knock. The  $\varepsilon$ - $\xi$  results are presented in Fig. 8.

The dependency of RoHR-u on ST changes and for the initial NO = 287 ppm is similar to the one presented in Fig. 6. The advancing of ST enhances the tendency for

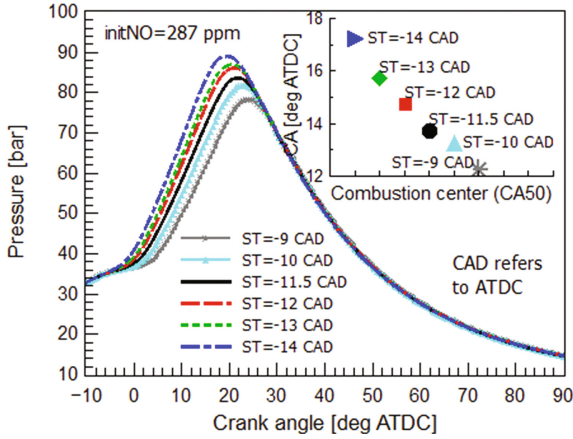


**Fig. 7.** Simulated in-cylinder pressure history and combustion center (CA50) for different ST values and constant NO content in the initial mixture (287 ppm) for OP2

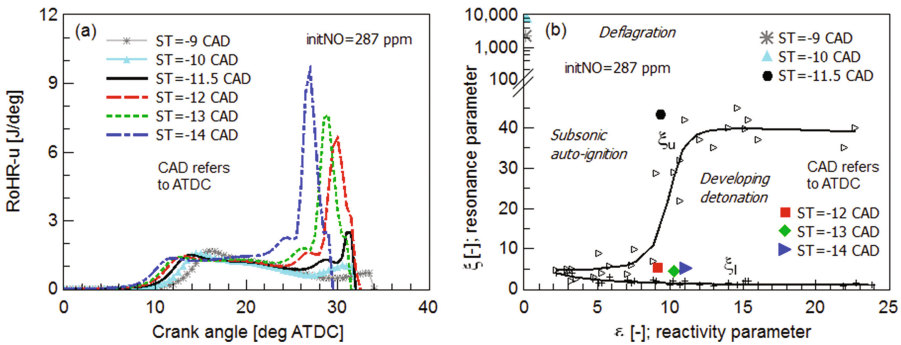


**Fig. 8.** RoHR-u histories (a) and the detonation peninsula from [28] along with the computed  $\epsilon$ - $\xi$  data (b) for different ST at constant initial NO content (287 ppm) in the mixture for OP2

auto-ignition, whereas the delaying of ST mitigates it. The change of ST has no significant impact on the maximum value of the first peak in the RoHR-u history. Only the position of maxima on a crank angle basis is different for different ST. Here, for the initial NO = 287 ppm the ST = -11.5 CAD ATDC corresponds to the operating of the engine at knock limit that is confirmed by the results in Fig. 8(b). The advancing of ST from -11.5 CAD ATDC by 0.5 CAD results in a transition from the regime of subsonic auto-ignition to the regime of developing detonation. Further advancing of ST moves the  $\xi$ - $\epsilon$  solution towards the lower limit of the resonance parameter ( $\xi_l$ ) and slightly higher values of the reactivity parameter ( $\epsilon$ ). On the contrary to that, the delaying of ST by 1.5 CAD or 2.5 CAD with reference to the value at knock limit (ST = -11.5 CAD ATDC) moves the  $\xi$ - $\epsilon$  solution towards very small values of  $\epsilon$  and very high values of  $\xi$  that are characteristic for deflagration (see Fig. 2).

#### 5.4 Influence of the Initial NO Content

The reduction of NO in the rest-gas is adopted in this work to avoid entering the detonation mode. The calculations refer to  $ST = -9$  CAD ATDC and are presented in Figs. 9 and 10.

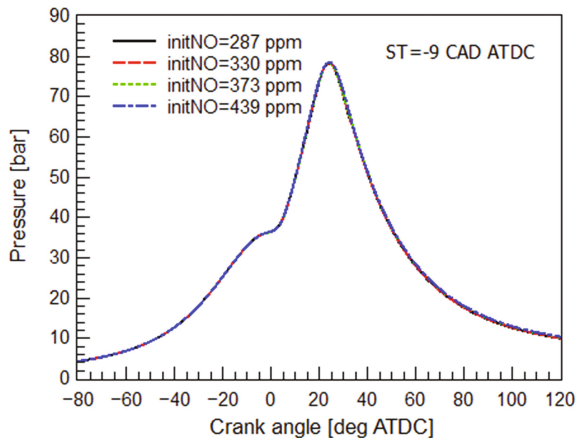


**Fig. 9.** Simulated pressure histories for different initial NO content in the in-cylinder mixture and at constant  $ST = -9$  CAD ATDC for OP2

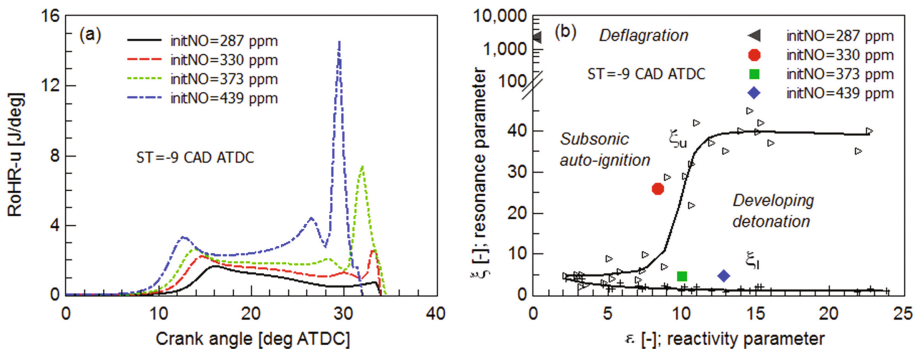


**Fig. 10.** Computed RoHR-u histories (a) and the detonation peninsula [28] along with the computed  $\varepsilon$ - $\xi$  data (b) for varied initial NO content in the mixture at  $ST = -9$  CAD ATDC for OP2

Varying only the initial NO content in the mixture between 287 ppm and 439 ppm has no impact on the combustion rate. The computed in-cylinder pressure histories overlap each other. A contrary situation is observed with respect to knocking tendency that is gained from the analysis of RoHR-u and the  $\xi$ - $\varepsilon$  solution in Fig. 10.

The rate of heat release in the unburned zone is very sensitive to the changes of NO in the rest-gas. Overall, by increasing NO, the reactivity of the mixture is enhanced that is revealed by significantly higher maximum values of the second peak of RoHR-u histories. Also the timing of the second peak of RoHR-u moves to earlier crank angle positions as the NO content increases, though the spark timing is unchanged. Furthermore, we also see the sensitivity of the first peak in the RoHR-u history. This is on the contrary to the impact of ST variation for a given constant NO content that is discussed in the previous section.

For the operating point investigated and for NO = 287 ppm there is only one peak recognized in the RoHR-u history that is attributed to low temperature chemistry. The lack of the second peak corresponds to very high  $\xi$  value (Fig. 10b) that for this combination of NO and ST indicates deflagration. Increasing NO to 330 ppm gives a rise the second peak in the RoHR-u. As a matter of fact, NO = 330 ppm and ST = -9 CAD ATDC correspond to the operation at knock limit that is discussed in Sect. 5.2. Further increasing of the NO content to 373 ppm and then to 439 ppm, result in high values of the second peak in the RoHR-u histories (Fig. 10a). These results are reflected in entering to the regime of developing detonation as it is shown in Fig. 10(b). Here, very small  $\xi$  and rather high  $\varepsilon$  values for these NO concentrations indicate knock of high severity.

## 5.5 Reduction of NO in the External EGR and ST Advancing

In the previous two sections we discuss separately from each other the impact of spark timing and the impact of reducing NO in the rest-gas on the combustion progress and knocking tendency. In order to avoid knocking combustion, spark timing must be delayed from its optimum position that results in less efficient combustion. The negative impact of the delayed spark timing can be compensated by reducing the NO content in the rest-gas that suppresses the end-gas auto-ignition and prevents a transition to knocking combustion.

The calculations in this section refer to OP2 that is also used for the analysis in previous sections. In the baseline configuration, which corresponds to the SRM calibrated to the experimental data, the ST is -9 CAD ATDC and the initial and total content of NO inside the cylinder is 330 ppm. This value corresponds to 12% of the rest-gas from which 7.9% is attributed to the external EGR. Such a distribution of the rest-gas was obtained during the preliminary analysis involving numerical simulations and measurements. Here, it is assumed that only NO that is contained in the external EGR can be reduced that corresponds to NO = 217 ppm. Overall, this can be understood as a cleaning of the recirculated gases as it has been recently shown in [16].

Starting from the baseline configuration, i.e. no reduction of NO in the external EGR and ST = -9 CAD ATDC, calculations are carried out for NO being reduced by 10%, 30%, 50%, 80% and 100%. This gives respectively, 330 ppm, 287 ppm, 221 ppm, 178 ppm, 134 ppm and 113 ppm of the total initial NO content in the mixture. For each content of NO, the ST is iteratively calibrated until the position is found that leads to the operation of the engine at knock limit. The knock limit is determined according to the method presented in Sect. 5.2. The results of the analysis



for each pair of NO and ST are presented in Fig. 11 with distinguishing between the engine operation at the knock limit (a, b) and just after it (c, d).

The results in Fig. 11 are qualitatively similar to those discussed in Sect. 5.2 – the advancing of ST by just 0.5 CAD causes a transition from a regular combustion mode to the mode of developing detonation. We note also a high sensitivity of the model for (1) NO = 134 ppm and ST = -17.5 CAD ATDC and for (2) NO = 178 ppm and ST = -16.5 CAD ATDC. For these two configurations and based on the  $\varepsilon$ - $\xi$  solutions in Fig. 11, the advancing of ST by 0.5 CAD causes a direct transition from the deflagration mode (Fig. 11a) to the detonation mode (Fig. 11b) and no solution is found in the subsonic regime. Furthermore, a shorter RoHR-u duration is recognized as the NO content decreases and ST is advanced (Fig. 11a, c).

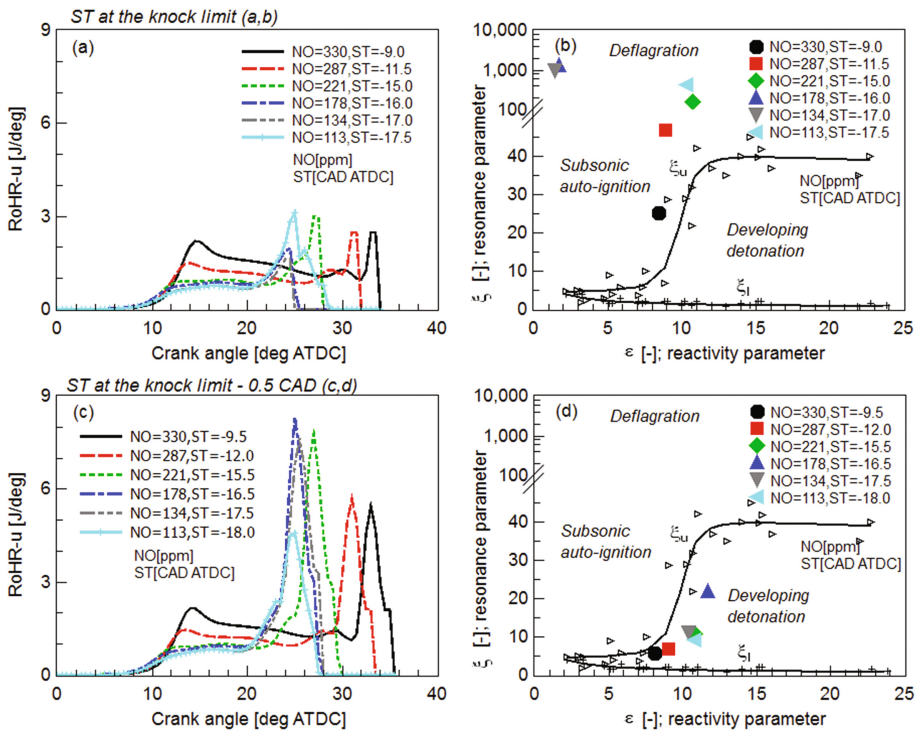


**Fig. 11.** Computed RoHR-u (a, c) and  $\varepsilon$ - $\xi$  solutions (b, d) in the detonation diagram from [28] for different pairs of initial NO content and ST positions at the knock limit (top row) and just after passing into the detonation mode (bottom row) due to the advancing of ST by 0.5 CAD

With respect to the combustion process (Fig. 12), the strongest impact of NO reduction for a given ST position is observed between 178 ppm and 330 ppm of the total NO content in the initial mixture. This corresponds to the 70% reduction of NO in the external EGR from 217 ppm to 65 ppm; the content of NO associated with the internal rest-gas (4%) remains constant. The impact of NO reduction is revealed by fast

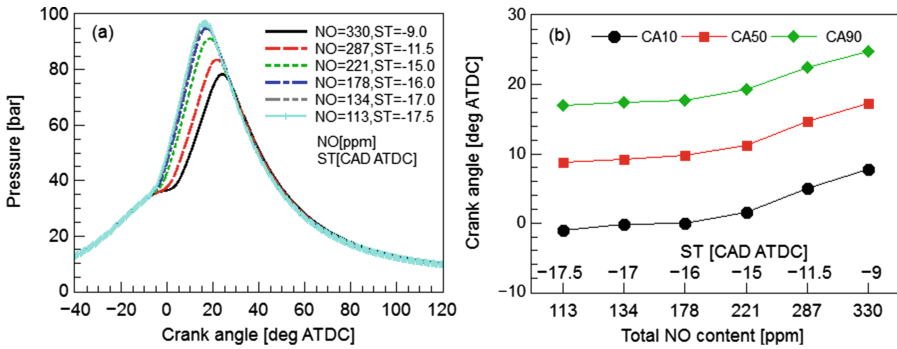


**Fig. 12.** The impact of NO reduction in the rest-gas and ST advancing on the in-cylinder pressure (a) and combustion progress (b) for the engine operated at OP2 and knock limit

advancing of CA10, CA50 and CA90 as well as higher maximum values of the in-cylinder pressure. Further reduction of NO does not have such a strong impact. The in-cylinder pressure histories for NO = 178 ppm, NO = 134 ppm and for 113 ppm are close to each other. The same tendency is observed for CA10, CA50 and CA90.

The results presented in Fig. 12 find reflection in the results plotted in Fig. 13 that contains the predicted IMEP, indicated specific fuel consumption (ISFC) and knock margin improvement.

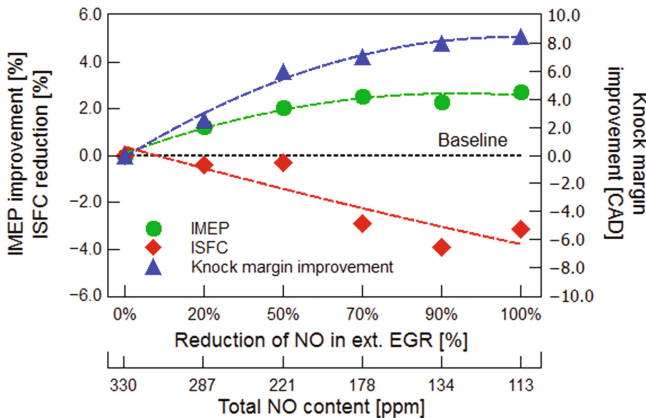


**Fig. 13.** The impact of NO reduction in the initial in-cylinder mixture on improving knock margin and fuel economy for OP2 (n = 4750 rpm, IMEP = 17 bar)

The dotted line in Fig. 13 represents the baseline solution that was obtained for ST = -9 CAD ATDC and NO = 330 ppm. The performance results in Fig. 13, such as IMEP, ISFC and knock margin improvement, are presented versus the total content of NO in the in-cylinder mixture and versus the percentage reduction of NO from the

external EGR. For the operating point investigated, the complete reduction of NO in the external EGR reduces the total NO content in the rest-gas by 66%. This reduction enables to advance the ST from the baseline value ( $ST = -9$  CAD ATDC) to  $ST = -17.5$  CAD ATDC and without the risk of knock occurrence (see Fig. 11a, b). The knock margin, which is calculated as a difference between the current ST and the baseline  $ST = -9$  CAD ATDC, is improved by 8.5 CAD and results in 3.2% reduction of ISFC. Similarly as in the results in Fig. 12, here the strongest impact of lowering NO on the knock margin improvement is observed up to 70% reduction of NO in the external EGR.

The results in Fig. 13 are an outcome of the numerical analysis that has not been verified directly by measurements. Therefore, it is very important to note here that the computed improvement of knock margin by 8.5 CAD would be very difficult, if not possible at all, to realize in practical applications. It would require a very precise control of the gas composition as well as very precise control and determination of knock-limited operation. As a consequence of this, the computed IMEP and ISFC are also expected to be lower in the actual engine operation than these here predicted. Nevertheless, an overall tendency of the presented computations looks sound. Confirmation of it is given by the existing experimental works. In [16], it is presented that the complete reduction of  $NO_x$  from the external EGR moves the combustion center towards an earlier position by 2 CAD. In [17], a complete reduction of  $NO_x$  from the initial mixture resulted in 6 CAD improvement of knock margin for 20% EGR and 3 CAD improvements for 10% EGR. These values correspond to 4.5% and 2.5% reduction of fuel consumption, respectively. The results in this article represent the same order of magnitude and therefore are considered plausible. As a consequence, the overall simulation methodology is also sound.

## 6 Summary

This paper reports a computational study about knocking tendency for an engine operated at high speed and load and with predefined EGR composition. Specifically, the impact of lowering the NO content in the initial in-cylinder mixture on knock onset along with the impact of advancing the spark timing to improve fuel economy are discussed. The investigations refer to the engine operated at  $n = 4750$  rpm and  $IMEP = 17$  bar. They are carried out using the SRM of engine in-cylinder processes that employs a detailed reaction kinetic model for the analysis of the end-gas auto-ignition process.

A combination of the SRM solution along with the evaluation of auto-ignition in the unburned zone and based on the detonation diagram provides a modeling framework that enables an efficient analysis of knocking tendency in SI engines. Not only the occurrence of auto-ignition is determined but also its severity that in consequence may give rise to the development of knock. Similarly as in our previous work [24], here it is also confirmed that this methodology can be used to determine the knock-limited engine operating conditions.

For the conditions investigated in this work, a comparison between the RoHR-u histories and the  $\xi$ - $\varepsilon$  solutions on the detonation diagrams indicate that the

knock-limited conditions correspond usually to the occurrence of two peaks in the RoHR-u that are of the same height. Thus, the RoHR-u results can be used for very first and rough estimation of the end-gas conditions with respect to knock occurrence. However, the assessment whether the auto-ignition may or may not give rise to knock can only be gained from the  $\xi$ - $\varepsilon$  solution.

Similarly as found in experimental works (see, e.g. [16, 17]) here it is also proved that the presence of NO in the mixture has a strong impact on knock onset. Specifically, by lowering the NO content the knock margin can be improved. For the conditions investigated in this work, a complete reduction of NO in the external EGR enabled the advancing of spark timing by 8.5 CAD with reference to the baseline position and without violating knock limit. The improvement of the knock margin results in 3.2% reduction of ISFC. The strongest impact of lowering NO on the knock margin improvement and ISFC reduction is observed up to 70% reduction of NO in the external EGR.

Although the obtained improvement of knock margin and ISFC have not been confirmed by measurements yet, they agree qualitatively to existing publications. Therefore, they are considered plausible and indicate the potential of cleaned EGR to improve fuel economy of gasoline engines. Furthermore, also the overall simulation methodology presented in this work is sound.

## Notation

ATDC	after top dead center
CA/CAD	crank angle/crank angle degree
CA10,50,90	crank angle of 10%, 50% and 90% of the cumulative heat release
CFD	computational fluid dynamics
EGR	exhaust gas recirculation
EVO	exhaust valve opening
IMEP	indicated mean effective pressure
ISFC	indicated specific fuel consumption
IVC	intake valve closure
OP	operating point
PS	pressure signal in knock detection using KIS4 from IAV
RoHR	rate of heat release
RoHR-u	rate of heat release in the unburned zone
SI	spark ignition
ST	spark timing
$C\phi$	mixing time constant
$l_I$	integral length scale of the flow
$n$	engine speed
$u'$	velocity fluctuation
$S_L$	laminar flame speed
$S_T$	turbulent flame speed
$\varepsilon$	reactivity parameter

$\tau$	scalar mixing time
$\tau_i$	ignition delay time
$\tau_e$	excitation time
$\tau_t$	turbulent mixing time
$\xi$	resonance parameter

## References

1. Heywood, J.B.: *Internal Combustion Engine Fundamentals*. McGraw-Hill, New York (1988)
2. Zhen, X., Wang, Y., Xu, S., Zhu, Y., Tao, C., Xu, T., Song, M.: The engine knock analysis – an overview. *Appl. Energ.* **92**, 628–636 (2012)
3. Rechs, M.: *Untersuchungen von Zylinderdruck- und Motorstrukturschwingungen zur Auslegung von Antiklopf-Regelsystemen*, Dissertation, RWTH Aachen (1990)
4. König, G.: *Auto-ignition and Knock Aerodynamics in Engine Combustion*, Dissertation, Leeds University (1993)
5. Chen, L., Li, T., Yin, T., Zheng, B.: A predictive model for knock onset in spark-ignition engines with cooled EGR. *Energy Convers. Manage.* **87**, 946–955 (2014)
6. Wang, Z., Liu, H., Reitz, R.D.: Knocking combustion in spark-ignition engines. *Prog. Energ. Combust.* **61**, 78–112 (2017)
7. Merola, S.S., Vaglieco, B.M.: Knock investigation by flame and radical species detection in spark ignition engine for different fuels. *Energy Convers. Manage.* **48**(11), 2897–2910 (2007)
8. Bozza, F., De Bellis, V., Teodosio, L.: Potentials of cooled EGR and water injection for knock resistance and fuel consumption improvements of gasoline engines. *Appl. Energ.* **169**, 112–125 (2016)
9. Netzer, C., Seidel, L., Pasternak, M., Mauss, F., Lehtiniemi, H., Ravet, F.: 3D CFD engine knock prediction and evaluation based on detailed chemistry and detonation theory. *Ber. Energie Verfahrenstechnik (BEV)* **17**(1), 185–196 (2017). ISBN 978-3-945806-08-1
10. Alger, T., Mangold, B.: Dedicated EGR: a new concept in high efficiency engines. *SAE Int. J. Engines* **2**(1), 620–631 (2009)
11. Prabhu, S.K., Li, H., Miller, D.L., Cernansky, N.P.: The effect of nitric oxide on autoignition of a primary reference fuel blend in a motored engine. *SAE Technical Paper 932757* (1993)
12. Amano, T., Dryer, F.L.: Effect of dimethyl ether, NO<sub>x</sub> and ethane on CH<sub>4</sub> oxidation: high pressure, intermediate temperature experiments and modeling. *Proc. Comb. Inst.* **27**, 397–404 (1998)
13. Kawabata, Y., Sakonji, T., Amano, T.: The effect of NO<sub>x</sub> on knock in spark-ignition engines. *SAE Technical Paper 1999-01-0572* (1999)
14. Stenlås, O., Gogan, A., Egnell, R., Sundén, B., Mauss F.: The influence of nitric oxide on the occurrence of autoignition in the end gas of spark ignition engines. *SAE Technical Paper 2002-01-2699* (2002)
15. Hoffmeyer, H., Montefrancesco, E., Beck, L., Willand, J., Ziebert, F., Mauss, F.: CARE – catalytic reformed exhaust gases in turbocharged DISI-engines. *SAE Int. J. Fuels Lubr.* **2** (1), 139–148 (2009)
16. Fischer, M., Kreutziger, P., Sun, Y., Kotrba, A.: Clean EGR for gasoline engines – innovative approach to efficiency improvement and emissions reduction simultaneously. *SAE Technical Paper 2017-01-0683* (2017)

17. Takaki, D., Tsuchida, H., Kobara, T., Akagi, M. et al.: Study of an EGR system for downsizing turbocharged gasoline engine to improve fuel economy. SAE Technical Paper 2014-01-1199 (2014)
18. Poschl, M., Sattelmayer, T.: Influence of temperature inhomogeneities on knocking combustion. *Combust Flame* **153**, 562–573 (2008)
19. LOGE AB. LOGEfuel gasoline v1.04, LOGEsoft v1.0, LOGEengine v1.0, software manuals (2017). <http://www.logesoft.com>
20. Pasternak, M., Mauss, F., Xavier, F., Riess, M., Sens, M., Benz, A.: 0D/3D simulations of combustion in gasoline engines operated with multi spark plug technology. SAE Technical Paper 2015-01-1243 (2015)
21. Pasternak, M., Mauss, F.: Sens., M., Riess, M., Benz, A., Stapf, K.G.: Gasoline engine simulations using zero-dimensional spark ignition stochastic reactor model and three-dimensional computational fluid dynamics engine model. *Int. J. Engine Res.* **17**(1), 76–85 (2016)
22. Peters, N.: *Turbulent Combustion*. Cambridge University Press, Cambridge (2000)
23. Pope, S.: Pdf methods for turbulent reactive flows. *Prog. Energ. Combust* **11**(2), 119–192 (1985)
24. Netzer, C., Seidel, L., Pasternak, M., Klauer, C., et al.: Engine knock prediction and evaluation based on detonation theory using a quasi-dimensional stochastic reactor model. SAE Technical Paper 2017-01-0538 (2017). <https://doi.org/10.4271/2017-01-0538>
25. Fischer, M., Günther, M., Röpke, K., Lindemann, M., Placzek, R.: Knock Detection in Spark-Ignition Engines. *MTZ Worldwide* 3/2003, vol. 64 (2003)
26. Stahr, A., Langfritz, P., Günther, M., Kratzsch, M.: The DELTA knocking control – the necessary paradigm shift for engines with high power density. In: *Proceedings 3rd Conference on “SI Engine Knock – Irregular Combustion”*, Berlin (2013)
27. Pilling, M.J.: Low-temperature combustion and autoignition. In: Hancock, G., Compton, R. G. (eds.) *Comprehensive Chemical Kinetics*, vol. 35, pp. 1–794. Elsevier, Amsterdam (1997)
28. Bradley, D., Morley, C., Gu, X., Emerson, D.: Amplified pressure waves during autoignition: relevance to CAI engines. SAE Technical Paper 2002-01-2868 (2002)
29. Zeldovich, Y.: Regime classification of an exothermic reaction with nonuniform initial conditions. *Combust. Flame* **39**, 211–214 (1980)
30. Bradley, D., Kalghatgi, G.T.: Influence of autoignition delay time characteristics of different fuels on pressure waves and knock in reciprocating engines. *Combust. Flame* **156**, 2307–2318 (2009)
31. Gu, X.J., Emerson, D.R., Bradley, D.: Modes of reaction front propagation from hot spots. *Combust. Flame* **133**, 63–74 (2003)
32. Kalghatgi, G.T., Bradley, D.: Pre-ignition and ‘super-knock’ in turbocharged spark-ignition engines. *SAE Int. J. Engines* **13**(4), 399–414 (2012)
33. Peters, N., Kerschgens, B., Paczko, G.: Super-knock prediction using a refined theory of turbulence. *SAE Int. J. Engines* **6**(2), 953–967 (2013)
34. Pan, J., Shu, G., Wei, H.: Interaction of flame propagation and pressure waves during knocking combustion in spark-ignition engines. *Combust. Sci. Techn.* **186**(2), 192–209 (2014)
35. Peters, N., Kerschgens, B., Jochim, B., Paczko, G.: Mega knock in super-charged gasoline engines interpreted as a localized developing detonation. In: Kratzsch, M., Guenther, M. (eds.) *Knocking in Gasoline Engines*. IAV Automotive Engineering, Berlin (2013)
36. Bates, L., Bradley, D., Paczko, G., Peters, N.: Engine hotspots: modes of auto-ignition and reaction propagation. *Combust. Flame* **166**, 80–85 (2016)